

Self-consistent Eliashberg theory, T_c , and the gap function in electron-doped cuprates

Dhananjay Dhokarh and Andrey V. Chubukov

Department of Physics, University of Wisconsin, Madison, Wisconsin 53706, USA

We consider normal state properties, the pairing instability temperature, and the structure of the pairing gap in electron-doped cuprates. We assume that the pairing is mediated by collective spin excitations, with antiferromagnetism emerging with the appearance of hot spots. We use a low-energy spin-fermion model and Eliashberg theory up to two-loop order. We justify ignoring vertex corrections by extending the model to $N \gg 1$ fermionic flavors, with $1/N$ playing the role of a small Eliashberg parameter. We argue, however, that it is still necessary to solve coupled integral equations for the frequency dependent fermionic and bosonic self-energies, both in the normal and superconducting state. Using the solution of the coupled equations, we find an onset of d -wave pairing at $T_c \sim 30$ K, roughly three times larger than the one obtained previously [P. Krotkov and A. Chubukov, Phys. Rev. B 74, 014509 (2006)], where it was assumed that the equations for fermionic and bosonic self-energies decouple in the normal state. To obtain the momentum and frequency dependent d -wave superconducting gap, $\Delta(\vec{k}_F, \omega_n)$, we derive and solve the non-linear gap equation together with the modified equation for the bosonic self energy which below T_c also depends on $\Delta(\vec{k}_F, \omega_n)$. We find that $\Delta(\vec{k}_F, \omega_n)$ is a non-monotonic function of momentum along the Fermi surface, with its node along the zone diagonal and its maximum some distance away from it. We obtain $2\Delta_{\max}(T \rightarrow 0)/T_c \sim 4$. We argue that the value of T_c , the non-monotonicity of the gap, and $2\Delta_{\max}/T_c$ ratio are all in good agreement with the experimental data on electron-doped cuprates.

PACS numbers:

I. INTRODUCTION

The first high temperature superconductors, discovered by Bednorz and Müller in 1986¹, were hole-doped cuprates, with Sr doped into La_2CuO_4 . Electron-doped cuprates were subsequently discovered in 1989, by doping Ce into Nd_2CuO_4 ². At present, there exist a variety of electron-doped cuprates of the form $\text{RE}_{2-x}\text{M}_x\text{CuO}_4$ where RE (rare earth lanthanides) is Nd or Pr and M is Ce or Th. For a comprehensive review on electron-doped cuprates see Ref.³.

Raman spectroscopy^{4,5} and ARPES⁶⁻⁹ provide strong evidence that the symmetry of the superconducting gap in both electron- and hole-doped cuprates is $d_{x^2-y^2}$. This gap symmetry is also consistent with tunnelling¹⁰, penetration depth¹¹⁻¹⁴, and Andreev reflections measurements¹⁵, although some of these experiments were originally interpreted differently. On the other hand, maximum T_c in electron-doped cuprates is in the range of 10 – 30 K, nearly an order of magnitude smaller than in hole-doped cuprates despite the ‘‘Hubbard U’’ being the same in both sets of materials (optical conductivity studies of parent hole- and electron-doped materials reported the same value, 1.7 eV, of the optical gap^{16,17}). Additionally, the d -wave gap in at least some electron-doped materials shows a non-monotonic behavior along the Fermi surface (FS), with the maximum somewhere in between the zone diagonal (where the gap vanishes) and the region near $(0, \pi)$ (Fig. 1). This non-monotonicity of the d -wave gap was predicted based on the analysis of Raman data⁴, and was subsequently measured directly by ARPES in $\text{Pr}_{0.89}\text{LaCe}_{0.11}\text{CuO}_4$ (Ref.⁹).

One way to obtain $d_{x^2-y^2}$ pairing is to assume that the

pairing is of electronic origin and is mediated by collective bosonic excitations at large momentum transfer, such that the interaction predominantly couples fermions with gaps of different signs (this effectively converts repulsive interaction into an attractive one). Both charge and spin fluctuations can give rise to such pairing. The idea of spin-fluctuation mediated pairing in cuprates has attracted substantial attention because antiferromagnetism is part of the phase diagram for both hole- and electron-doped cuprates. We follow earlier works on both hole and electron-doped cuprates¹⁸⁻²⁴ and other materials²⁵⁻²⁷, and consider spin-mediated pairing.

In this paper we consider two issues. First, the origin of the smallness of T_c in electron-doped cuprates compared to hole-doped cuprates; second, the momentum and frequency dependence of the superconducting gap.

The relative smallness of T_c in electron-doped cuprates is generally attributed to the fact that in these systems d -wave pairing is less effective because hot spots (points at the FS separated by the antiferromagnetic momentum $\vec{Q} = (\pi, \pi)$) are located much closer to the zone diagonals (see Fig. 1). This argument, however, is incomplete because magnetically-mediated T_c remains finite and scales linearly with the overall spin-fermion coupling, even when hot spots merge at the zone diagonals²⁸. The complete picture is that in electron-doped cuprates, T_c acquires the dependence of the FS curvature because the velocities of hot fermions become nearly antiparallel to each other when hot spots approach zone diagonals (Fig. 1). Krotkov and one of us²⁸ (hereafter referred to as KC) demonstrated that it is this dependence that gives rise to the additional numerical smallness of T_c . Using the same Eliashberg-type computational procedure as in

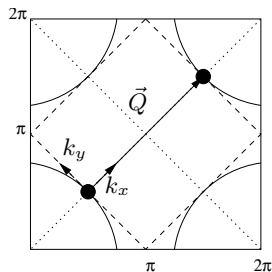


FIG. 1: Brillouin zone for electron-doped cuprates at the doping when hot spots merge on the zone diagonals. We argue that this doping is close to the one at which antiferromagnetic order emerges. The arcs represent the FSs, the dashed square represents the antiferromagnetic Brillouin zone. k_x and k_y are the directions of fermionic momenta transverse and along the FS, respectively.

hole-doped cuprates, KC obtained $T_c \sim 10$ K, using for the coupling the value extracted from the optical data at half-filling.

Compared to experiment, the value of 10 K is a bit small, particularly given that “hot spot constrained” calculations tend to somewhat overestimate T_c ²⁹.

In light of these points, we re-consider here the Eliashberg computational procedure. We argue that the earlier study neglected corrections of order one and should be therefore modified. To understand where the modification is required, we note that for superconductivity mediated by collective boson exchange Eliashberg-type calculations of T_c differ qualitatively from those of phonon-mediated superconductivity. For phonon superconductivity, the full phonon propagator is an input with the bosonic self-energy neglected because it is small by the same parameter as vertex corrections. For collective mode mediated pairing, bosonic dynamics originates from low-energy fermions and has to be computed together with the fermionic self-energy. As a consequence, one generally has to solve a coupled set of integral equations for the fermionic self-energy, $\Sigma(\vec{k}, \omega)$, and the bosonic self-energy (the bosonic polarization operator), $\Pi(\vec{q}, \Omega)$.

For hole-doped cuprates, the solution of this coupled set near hot spots is further simplified because bosonic self-energy, $\Pi(\vec{Q}, \Omega)$, has the form of Landau damping and does not depend on the fermionic self-energy. As a result, the set of coupled equations for $\Sigma(\omega) \equiv \Sigma(\vec{k}_{\text{hs}}, \omega)$ and $\Pi(\vec{Q}, \Omega)$ reduces to just one equation for $\Sigma(\omega)$, while $\Pi(\vec{Q}, \Omega)$ remains the same as for free fermions.

The reasoning for the independence of $\Pi(\vec{Q}, \Omega)$ from $\Sigma(\omega)$ is the following: $\Pi(\vec{Q}, \Omega)$ is a convolution of a particle and a hole, located near hot spots separated by \vec{Q} . When these two fermions have Fermi velocities directed at an arbitrary angle w.r.t. each other, each fermionic line can be integrated over its dispersion $\epsilon_{\mathbf{k}}$, $\epsilon_{\mathbf{k}+\mathbf{Q}}$, and $\Pi(\vec{Q}, \Omega)$ emerges as the convolution of the two

local propagators $\mathcal{G}_1(\omega) = \int d\epsilon_{\mathbf{k}} \mathcal{G}(\vec{k}, \omega)$ and $\mathcal{G}_1(\omega + \Omega) = \int d\epsilon_{\mathbf{k}+\mathbf{Q}} \mathcal{G}(\vec{k} + \vec{Q}, \omega + \Omega)$. The local $\mathcal{G}_1(\omega) = -i\pi \text{sgn}(\omega)$, and does not depend on fermionic $\Sigma(\omega)$; hence one does not need to dress up fermionic propagators. An alternate way to state this is to observe that Landau damping is an anomaly, i.e., it can be re-expressed as the contribution from high-energies, where fermions are free particles.

Applying Eliashberg approach to electron-doped cuprates, KC assumed that the equations for Σ and Π decouple in this case too, so that they used the free-fermion $\Pi(\vec{Q}, \omega)$ to compute $\Sigma(\omega)$ and T_c . However, $\Pi(\vec{Q}, \omega)$ for electron-doped cuprates scales as $\sqrt{|\Omega|}$ rather than as $|\Omega|$. This is because the Fermi velocities of hot fermions are anti-parallel, and the Jacobian of the transformation from $\int d^2\mathbf{k}$ to $\int d\epsilon_{\mathbf{k}} d\epsilon_{\mathbf{k}+\mathbf{Q}}$ diverges, so that $\Pi(\vec{Q}, \Omega)$ no longer reduces to the convolution of local propagators (alternatively, $\Pi(\vec{Q}, \Omega)$ is not an anomaly). As a consequence, $\Pi(\vec{Q}, \Omega)$ acquires the dependence on $\Sigma(\omega)$, and one has to solve the coupled set of equations for Σ and Π .

We found that to a good numerical accuracy, the solution of the coupled set modifies previous results of KC by a constant factor $\alpha \sim 0.6$. That is, $\Pi(\vec{Q}, \Omega)$ by α and Σ gets multiplied by $1/\sqrt{\alpha}$. Recalculating T_c using these rescaled quantities, we find that T_c increases by a factor $1/\alpha^2 \sim 3$. This brings Eliashberg T_c to 30 K, which is quite consistent with the experimental data.

This $T_c \sim 30$ K is also in better agreement with T_c obtained within the FLEX approximation²¹. In FLEX, full Green’s functions are used, but vertex corrections are neglected. The fact that for electron-doped cuprates we also need to use the full Green’s functions makes Eliashberg theory more of a match with FLEX than for hole-doped cuprates. Nevertheless, Eliashberg and FLEX are still not equivalent because in FLEX the full momentum dependent $\Sigma(\vec{k}, \omega)$ is used (and vertex corrections are neglected, though without any parametrical justification), while in our Eliashberg theory, only $\Sigma(\vec{k}_F, \omega)$ is relevant, while $d\Sigma(\vec{k}, \omega)/d\epsilon_{\mathbf{k}}$ and vertex corrections are neglected, by analogy with the electron-phonon problem. There is, however, no “natural” Eliashberg parameter analogous to ω_D/E_F , and to justify the approximation we need to extend the theory to N fermionic flavors and consider large N limit; then $1/N$ becomes the Eliashberg parameter.

Very recent studies³⁰ have demonstrated that the large N approximation in fact does not work beyond two-loop order. There are a series of multi-loop diagrams, beginning at three-loop order, which do not contain $1/N$, although apparently small numerically. We restrict to two-loop order, and do not address this issue in the present MS.

The second issue we consider is the form of the superconducting gap as a function of momentum along the Fermi surface. KC obtained a non-monotonic gap function by solving for the d -wave eigenfunction of the gap equation at T_c . Here we solve the non-linear gap equation for $T < T_c$ (together with the coupled equation for

the bosonic $\Pi(\vec{Q}, \Omega)$, and find that the gap remains non-monotonic for $T < T_c$; there is a slight change in shape with T , but the non-monotonic character remains intact. At $T \rightarrow 0$, we find that the maximum value of the gap along the FS, Δ_{\max} , is about two times larger than T_c , i.e., within Eliashberg theory, $2\Delta_{\max}/T_c \sim 4$. This ratio is quite consistent with these experimental data: from optics we have³¹ $2\Delta_{\max}/T_c \sim 5$ for $\text{Pr}_{1.85}\text{Ce}_{0.15}\text{CuO}_4$, and from Raman measurements⁵ on $\text{Pr}_{2-x}\text{Ce}_x\text{CuO}_4$ and $\text{Nd}_{2-x}\text{Ce}_x\text{CuO}_4$ we have $2\Delta_{\max}/T_c \sim 3.5$.

The paper is organized as follows. In Sec. II we briefly review the spin-fermion model for electron-doped cuprates and its extension to $N \gg 1$. In Sec. III we carry out normal state analysis. We show that vertex corrections are small by $1/N$, but that self-energy corrections to $\Pi(\vec{Q}, \Omega)$ are important. We then solve coupled equations for $\Sigma(\omega)$ and $\Pi(\vec{Q}, \Omega)$, and compare our results with those of KC, who used bare fermionic propagators to compute $\Pi(\vec{Q}, \Omega)$. We find that the fermionic self-energy scales as $(\bar{\omega}_0)^{1/4}|\omega|^{3/4}$, and we use this $\bar{\omega}_0$ scale as a measure for T_c . In Sec. IV we study the superconducting properties. We first solve for T_c , and then derive and solve the non-linear gap equation. The latter yields the non-monotonic d -wave gap $\Delta(\vec{k}_F, \omega_n)$, which depends on momentum along the FS and also on Matsubara frequency. Using this solution, we obtain the ratio $2\Delta_{\max}/T_c$. In Sec. V we summarize and discuss our results. A vertex correction calculation is relegated to the Appendix.

II. THE MODEL

Spin-fermion model has been discussed before, so we will be brief. The idea is that the low-energy physics of a system of itinerant fermions near antiferromagnetic instability, is adequately described by the interaction with low-energy, collective, bosonic excitations in the spin channel. The static part of a collective mode propagator comes from fermions at high energies and is the input for the low-energy theory, while the dynamical part comes from low-energy fermions and has to be calculated within the low-energy theory. The Hamiltonian of the spin-fermion model is

$$\begin{aligned} \mathcal{H} = & \sum_{\mathbf{k}} \epsilon_{\mathbf{k}} c_{\mathbf{k},\alpha}^\dagger c_{\mathbf{k},\alpha} + \sum_{\mathbf{q}} \chi_{\text{st}}^{-1}(\mathbf{q}) \mathbf{S}_{\mathbf{q}} \cdot \mathbf{S}_{-\mathbf{q}} \\ & + g \sum_{\mathbf{q}, \mathbf{k}, \alpha, \beta} c_{\mathbf{k}+\mathbf{q},\alpha}^\dagger \boldsymbol{\sigma}_{\alpha,\beta} c_{\mathbf{k},\beta} \cdot \mathbf{S}_{-\mathbf{q}} \end{aligned} \quad (1)$$

where $\epsilon_{\mathbf{k}}$ is the electronic dispersion, $c_{\mathbf{k},\alpha}$ is the fermionic operator for an electron with momentum \mathbf{k} and spin α , $\boldsymbol{\sigma}$ are the Pauli spin matrices, and $\mathbf{S}_{\mathbf{q}}$ is the bosonic variable describing collective spin degrees of freedom. Further, g is the coupling constant and $\chi_{\text{st}}(\mathbf{q})$ is the static spin susceptibility (the static propagator of collective spin degrees of freedom). The triple spin-fermion vertex is shown diagrammatically in Fig. 2. We will not

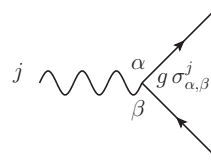


FIG. 2: The vertex for the spin-fermion interaction. The solid lines are fermions, the wavy line is a spin fluctuation.

show the spin indices explicitly in subsequent Feynman diagrams; it should be understood that they are there, and proper accounting of them has been done to calculate the various prefactors while translating the diagrams into equations.

For the static spin susceptibility, we follow earlier works and use the Ornstein-Zernike form

$$\chi_{\text{st}}(\vec{q}) = \frac{\chi_0}{\xi^{-2} + (q - Q)^2}, \quad (2)$$

where ξ is the magnetic correlation length. The constant χ should not be taken as another input because g and χ_0 only appear in the combination $\bar{g} = g^2 \chi_0$. Throughout the paper we refer to \bar{g} as the effective spin-Fermion coupling constant.

Numerical studies of the onset of antiferromagnetic instability all show that antiferromagnetism emerges around the doping when hot spots merge along zone diagonals and the Fermi surface touches the antiferromagnetic Brillouin zone, as shown in Fig. 1. The analytical argument is that the derivative of the static susceptibility of free fermions $\chi_{\text{st}}^0(Q)$ with respect to doping diverges at this point, so that in its near vicinity $U\chi_{\text{st}}^0(Q)$ reaches one and within RPA the full $\chi_{\text{st}}(Q) \propto 1/(1 - U\chi_{\text{st}}^0(Q))$ diverges. We assume for definiteness that the antiferromagnetic quantum critical point (QCP), at which $\xi^{-1} = 0$, is right at this doping. Our results will change only a little if ξ diverges not at this point, but close to it.

As mentioned in the Introduction, the velocities of the fermions along Brillouin zone diagonals are anti-parallel to each other, with the tangential component along the FS vanishing (see Fig. 1). The dispersion of fermions near the hot spots is then not the usual $\epsilon_{\mathbf{k}} = v_{Fx}k_x + v_{Fy}k_y$, but

$$\epsilon_{\mathbf{k}} = v_F k_x + \beta^2 k_y^2 \quad (3)$$

$$\epsilon_{\mathbf{k}+\mathbf{Q}} = -v_F k_x + \beta^2 k_y^2 \quad (4)$$

where β^2 parameterizes the curvature of the Fermi surface; this will play an important role in our analysis.

It is convenient to measure the combined effect of the curvature and the interaction in terms of the dimensionless parameter

$$r = \frac{\bar{g}\beta^2}{\pi v_F^2} \quad (5)$$

For parameters relevant to electron-doped cuprates, $r \sim 10^{-1}$. We also introduce for further use, the momentum scale

$$q_0 = \frac{\bar{g}}{\pi v_F} \quad (6)$$

and the frequency scale

$$\omega_0 = \left(\frac{\bar{g}\beta}{2\pi v_F} \right)^2 = \left(\frac{q_0\beta}{2} \right)^2 = \frac{\bar{g}r}{4\pi} \quad (7)$$

The computational procedure is straightforward. We need to obtain the dynamic spin susceptibility, $\chi(\vec{q}, \Omega_n)$, in which the frequency dependence comes through the total polarization operator $\Pi_{\text{tot}}(\vec{q}, \Omega_n)$, which contains contributions from both umklapp and non-umklapp processes. We have

$$\chi(\vec{q}, \Omega_n) = \frac{\chi_0}{(q - Q)^2 + \chi_0 \Pi_{\text{tot}}(\vec{q}, \Omega_n)} \quad (8)$$

where

$$\Omega_n = 2n\pi T \quad (9)$$

is a Bosonic Matsubara frequency, and

$$\Pi_{\text{tot}}(\vec{q}, \Omega_n) = 2(\Pi(\vec{q}, \Omega_n) + \Pi(-\vec{q}, \Omega_n)) \quad (10)$$

We also need to obtain the full normal and anomalous Green's functions $\mathcal{G}(p)$ and $\mathcal{F}(p)$, respectively. These depend on the normal and anomalous self-energies, Σ and Σ_{02} , as

$$\begin{aligned} \mathcal{G} &= \frac{X(-p)}{X(-p)X(p) + (\Sigma_{02}(p))^2} \\ \mathcal{F} &= \frac{\Sigma_{02}(p)}{X(-p)X(p) + (\Sigma_{02}(p))^2} \end{aligned} \quad (11)$$

where $p = (\vec{p}, \omega_n)$, $\omega_n = \pi T(2n + 1)$ is a fermionic Matsubara frequency, and

$$X(p) \equiv \mathcal{G}_0^{-1}(p) + \Sigma(p), \quad \mathcal{G}_0^{-1}(p) = i\omega_n - \epsilon_{\vec{p}}. \quad (12)$$

In Eliashberg approximation, which we justify below, the normal and anomalous fermionic self-energies are given by one-loop diagrams (Fig. 3) that generally involve the full fermionic propagators and the full dynamical spin susceptibility; similarly, the bosonic self-energy, $\Pi(\vec{q}, \Omega_n)$, is the sum of bubbles made of the full fermionic propagators (Fig. 4). We have,

$$\begin{aligned} \Sigma(p) &= -3g^2T \sum_m \int \frac{d^2\vec{k}}{(2\pi)^2} \mathcal{G}(\vec{k}, \omega_m) \chi(\vec{k} - \vec{p}, \omega_m - \omega_n) \\ \Sigma_{02}(p) &= -3g^2T \sum_m \int \frac{d^2\vec{k}}{(2\pi)^2} \mathcal{F}(\vec{k}, \omega_m) \chi(\vec{k} - \vec{p}, \omega_m - \omega_n) \end{aligned} \quad (13)$$

$$\begin{aligned} \Pi(\vec{q}, \Omega_n) &= 2g^2T \sum_m \int \frac{d^2\vec{k}}{(2\pi)^2} \left(\mathcal{G}(\vec{k}, \omega_m) \mathcal{G}(\vec{k} + \vec{q}, \omega_m + \Omega_n) \right. \\ &\quad \left. + \mathcal{F}^\dagger(\vec{k}, \omega_m) \mathcal{F}(\vec{k} + \vec{q}, \omega_m + \Omega_n) \right) \end{aligned} \quad (14)$$

These equations can be further simplified by integrat-

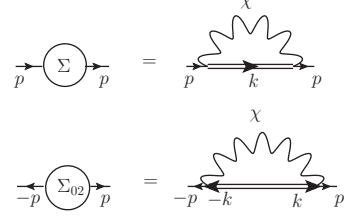


FIG. 3: Diagrams for the normal and anomalous fermionic self-energies (Σ and Σ_{02} , respectively) in the Eliashberg-type theory (no vertex corrections). The double lines are full Green's functions of intermediate fermions, with self-energies included.

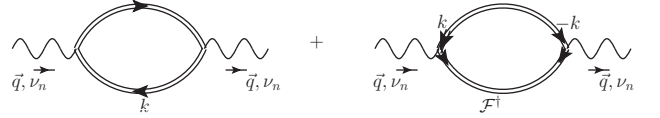


FIG. 4: Diagrams for the polarization operator. The diagram on the right is present only in the superconducting state.

ing the r.h.s. over $\epsilon_{\mathbf{k}}$. The dependence on $\epsilon_{\mathbf{k}}$ is in both fermionic and bosonic propagators, but the one in the bosonic propagator can be neglected because overdamped bosons are slow modes compared to fermions; keeping the dependence on $\epsilon_{\mathbf{k}}$ in χ , only gives rise to a small correction in the Eliashberg parameter. Within the Eliashberg approximation, we also neglect the dependence of the fermionic self-energies on $\epsilon_{\mathbf{k}}$. With these steps the integration over $\epsilon_{\mathbf{k}}$ is straightforward. For the normal state self-energy at a finite temperature we have

$$\begin{aligned} \Sigma(k_y, \omega_n) &= \frac{i3g^2T}{4\pi v_F} \text{sgn}(\omega_n) \times \\ &\quad \sum_{|\Omega_m| < |\omega_n|} \int_{-\infty}^{\infty} dp_y \chi(k_y, p_y, \Omega_m) \end{aligned} \quad (15)$$

where k_y is the momentum component along the FS ($v_F k_x = -\beta^2 k_y^2$) and $\chi(k_y, p_y, \Omega_m) = \chi(\vec{k} - \vec{p}, \Omega_m)|_{\epsilon_{\mathbf{k}} = \epsilon_{\mathbf{p}} = 0}$ is the spin susceptibility at momenta connecting two points on the FS. Similarly, the linearized equation for the anomalous self-energy, valid at $T = T_c$, is

$$\begin{aligned} \Sigma_{02}(k_y, \omega_n) &= -\frac{3g^2T}{4\pi v_F} \sum_m \int dp_y \frac{\chi(k_y, p_y, \omega_m - \omega_n)}{|\omega_m + i\Sigma(p_y, \omega_m)|} \times \\ &\quad \Sigma_{02}(p_y, \omega_m) \end{aligned} \quad (16)$$

We assume d -wave pairing for which $\Sigma_{02}(k_y, \omega_n) = -\Sigma_{02}(k_y + \vec{Q}, \omega_n)$. Shifting p_y by \vec{Q} in Eqs. (15) and (16), we eliminate the overall minus sign on the r.h.s. of (16). The polarization operator becomes, after the shift, $\Pi_{\text{tot}}(\vec{k} - \vec{p} - \vec{Q}, \Omega)$ and can be approximated by $\Pi_{\text{tot}}(\vec{Q}, \Omega) = 4\Pi(\vec{Q}, \Omega)$. The susceptibility spin susceptibility, $\chi(k_y, p_y, \Omega)$, then takes the form

$$\chi(k_y, p_y, \Omega_m) = \frac{\chi_0}{(k_y - p_y)^2 + (\beta^2/v_F)^2(k_y^2 + p_y^2)^2 + 4\chi_0\Pi(\vec{Q}, \Omega_m)} \quad (17)$$

$$= \frac{\chi_0}{q_0^2 \left((k - p)^2 + r^2(k^2 + p^2)^2 + \frac{4\chi_0}{q_0^2}\Pi(\vec{Q}, \Omega_m) \right)}$$

As mentioned in the Introduction, for fermion-fermion interaction mediated by a collective mode, there is no natural small Eliashberg-type parameter, analogous to ω_D/E_F , that would make vertex corrections and $d\Sigma(k)/d\epsilon_k$ much smaller than one. To rigorously justify Eliashberg approximation, we need to extend the theory to $N > 1$ fermionic flavors and take the $N \gg 1$ limit. Applying this extension to the low-energy model of Eq. (1), we find that the polarization operator acquires an overall factor of N . This factor also appears in the normal state fermionic self-energy, and can be absorbed into the renormalization of the frequency scale ω_0 (given by Eq. (7)), by redefining,

$$\omega_0 \rightarrow \frac{\omega_0}{N^2} \quad (18)$$

Throughout the paper we will use this redefined ω_0 , keeping it fixed by rescaling the curvature β by N .

III. NORMAL STATE ANALYSIS

We begin by citing the results from Ref. 28 for the normal state polarization operator and the normal state fermionic self-energy at the hot spot, obtained without self-consistency. The polarization operator is given by

$$\Pi_0(\vec{Q}, \Omega_n) = \frac{Ng^2}{2\pi\beta v_F} \sqrt{|\Omega_n|} F_{\Pi} \left(\frac{T}{|\Omega_n|} \right) \quad (19)$$

where $F_{\Pi}(x \rightarrow 0) = 1$, $F_{\Pi}(x \gg 1) \sim \sqrt{x}$, and the subscript 0 is used to emphasize that Π_0 is obtained using bare fermionic propagators. The fermionic self-energy at the hot spot is given by

$$\Sigma(\omega_n) = i(\omega_0)^{1/4} |\omega_n|^{3/4} \text{sgn}(\omega_n) F_{\Sigma} \left(\frac{|\omega_n|}{\omega_0^N} \right) \quad (20)$$

where $F_{\Sigma}(x \ll 1) \propto x^{0.1}$ and $F_{\Sigma}(x \gg 1) \approx 1$. For the pairing problem we need the region $|\omega_n| \geq \omega_0$, for which F_{Σ} can be approximated reasonably well by one.

We now discuss how these results are modified when we go beyond bare vertices and free fermion propagators. For definiteness, for the rest of this section we restrict our analysis to $T \rightarrow 0$.

A. Vertex corrections

We first show that diagrams with vertex corrections are small by $1/N$. As an example, consider the vertex correction diagram for the polarization operator (Fig. 5). We have

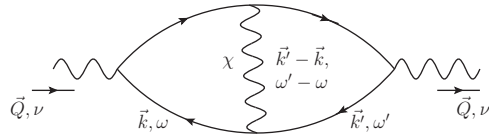


FIG. 5: The polarization operator with the vertex correction, but without self-energy corrections to intermediate fermions.

$$\Pi_v(\vec{Q}, \Omega) = -2Ng^4 \int_{-\infty}^{\infty} \frac{d\omega d^2\mathbf{k}}{(2\pi)^3} \frac{d\omega' d^2\mathbf{k}'}{(2\pi)^3} \mathcal{G}(\vec{k}, \omega) \times \mathcal{G}(\vec{k} + \vec{Q}, \omega + \Omega) \mathcal{G}(\vec{k}', \omega') \mathcal{G}(\vec{k}' + \vec{Q}, \omega' + \Omega) \chi(\vec{k} - \vec{k}', \omega - \omega') \quad (21)$$

where the subscript v stands for Π with vertex correction. The calculation is presented in Appendix A, and the result is

$$\Pi_v(\vec{Q}, \Omega) = \frac{g^2}{4\pi\beta v_F} \sqrt{\frac{\Omega}{8}} \log \left(4\sqrt{2}N^2 \sqrt{\frac{\omega_0}{\Omega}} \right) \quad (22)$$

Comparing this with the result for $\Pi_0(\vec{Q}, \Omega)$ (Eqn (19)), we immediately see that

$$\frac{\Pi_v}{\Pi_0} = \frac{\log(4\sqrt{2}N^2 \sqrt{\frac{\omega_0}{\Omega}})}{4\sqrt{2}N}, \quad (23)$$

i.e., the vertex correction diagram for the polarization operator contains additional $\log N/N$ and can be safely neglected at large N . One can verify that the same is true with the vertex correction diagram for the fermionic self-energy.

B. Self-energy corrections to the polarization operator Π

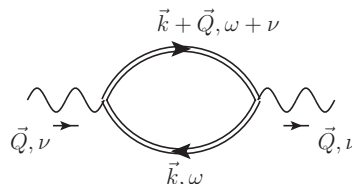


FIG. 6: The polarization operator without vertex corrections, but with full propagators of intermediate fermions.

We next show that corrections from inserting self-energy into the fermionic lines in the particle-hole bubble are not small in $1/N$ and should be included. For this, we evaluate the polarization bubble $\Pi_{\text{se}}(\vec{Q}, \Omega)$ at $T \rightarrow 0$ with the renormalized Green's functions (Fig. 6) and compare the result with $\Pi_0(\vec{Q}, \Omega)$. We discuss full self-consistency later. The Green's function used is,

$$\mathcal{G}(\vec{k}, \omega_n) = \frac{1}{i(\omega_n + s(\omega_n)\text{sgn}(\omega_n)) - \epsilon_{\vec{k}}} \quad (24)$$

where

$$s(\omega_n) = (\omega_0)^{1/4} |\omega|^{3/4} \quad (25)$$

For the diagram for Π_{se} we have

$$\Pi_{\text{se}}(\vec{Q}, \Omega) = 2Ng^2 \int_{-\infty}^{\infty} \frac{d\omega d^2\mathbf{k}}{(2\pi)^3} \frac{1}{(\epsilon_{\vec{k}} - i(\omega + s(\omega)\text{sgn}(\omega)))(\epsilon_{\vec{k}+\vec{Q}} - i(\omega + \Omega + s(\omega + \Omega)\text{sgn}(\omega + \Omega)))} \quad (26)$$

Expanding the dispersion around the hot spots, carrying out the integration over momenta, rescaling the resulting expression, and subtracting the zero frequency contribution (the static part is already absorbed in $\chi_{\text{st}}^0(\vec{Q})$), we obtain

$$\begin{aligned} \Pi_{\text{se}}(\vec{Q}, \Omega) &= \frac{g^2 N}{2\pi\beta v_F} \sqrt{\Omega} I\left(\frac{\Omega}{\omega_0}\right) \\ &= \Pi_0(\vec{Q}, \Omega) I\left(\frac{\Omega}{\omega_0}\right), \end{aligned} \quad (27)$$

where

$$\begin{aligned} I(x) &= -\frac{1}{\sqrt{x}} \left(\int_0^{\infty} \frac{dy}{\sqrt{2y + x + y^{3/4} + (x+y)^{3/4}}} \right. \\ &\quad \left. - \int_0^{\infty} \frac{dy}{\sqrt{2y + 2y^{3/4}}} \right) \end{aligned} \quad (28)$$

We plot $I(x)$ in Fig. 7. This function monotonically in-

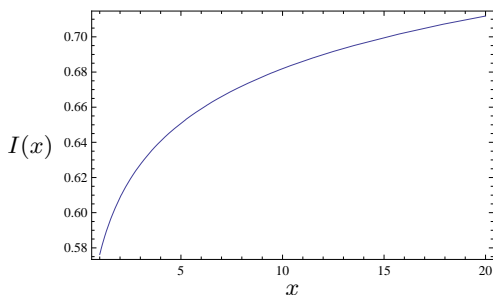


FIG. 7: Plot of the function $I(x)$ given by Eqn. (28) vs. $x = \Omega/\omega_0$ for $x > 1$. Observe that $I(x)$ changes little between $x = 1$ and $x \sim 10$. At very large x , $I(x)$ approaches one.

creases with x and approaches one at large x . This limiting behavior can be easily extracted from the integral for $I(x)$.

We see that $\Pi_{\text{se}}(\vec{Q}, \Omega)$ is of the same order as $\Pi_0(\vec{Q}, \Omega)$, i.e., there is no factor $1/N$ between them. This is not

surprising as for typical $\Omega \sim \omega_0$ (i.e., for typical $x \sim O(1)$ in $I(x)$), ω and $\Sigma(\omega)$ are of the same order. This is in contrast to the vertex correction diagram in which the insertion of an additional bosonic propagator adds a $1/N$ factor. This factor could potentially be compensated by additional powers of momentum and frequency in the denominator; however it turns out that the integration over momentum and frequency in the diagram for Π_{v} only adds an additional $\log N$.

We therefore conclude that it is possible to ignore vertex corrections; but two-loop self-energy corrections to the polarization operator cannot be ignored. Therefore, we do need to calculate $\Sigma(\omega)$ and $\Pi(\vec{Q}, \Omega)$ self-consistently. In this respect, the calculation of Σ and Π in electron-doped cuprates is qualitatively different from that in hole-doped cuprates, where $\Pi(\vec{Q}, \Omega) \propto |\Omega|$ does not depend on Σ , i.e., the equations for Σ and Π decouple.

We discuss our self-consistent solution in the next subsection.

C. Self-consistent analysis of $\Sigma(\omega)$ and $\Pi(\vec{Q}, \Omega)$

For the self-consistent calculation of the bosonic self-energy, Π , and the normal state fermionic self-energy, $\Sigma(\omega)$, we use equations (15), (17), and the diagram in Fig. 6. In general, this would require one to solve the resulting coupled integral equations. In our case however, there is a way to simplify this calculation because the function $I(x)$ in (28) is quite flat at $x \geq 1$, varying only by 8% between $x = 1$ and $x = 5$ (roughly from 0.6 to 0.65). To a reasonable accuracy, we can then approximate $I(x)$ by a constant $\alpha \sim 0.6$. Once we make this approximation, the polarization operator, Π , can be cast into the form

$$\Pi_{\text{se}}(\vec{Q}, \Omega) = \frac{q_0^2}{4\chi_0} \sqrt{\Omega/\omega_0} \quad (29)$$

where

$$\bar{\omega}_0 = \frac{\omega_0}{\alpha^2} \quad (30)$$

In other words, the dressed Π_{se} differs from Π_0 in Eq. (19) by the replacement $\omega_0 \rightarrow \bar{\omega}_0$, without changing q_0 . Because $\omega_0 = q_0^2 \beta^2 / 4$, this renormalization implies that the curvature β gets effectively renormalized into $\bar{\beta} = \beta / \alpha$. Substituting this polarization operator into equation (15) for the self-energy, we obtain, for $\omega > \bar{\omega}_0$,

$$\begin{aligned} \Sigma(\omega) &= i \frac{3\bar{g}}{4\pi^2 v_F q_0} \text{sgn}(\omega) \int_0^{|\omega|} d\Omega \int_{-\infty}^{\infty} \frac{dk}{\left(k^2 + \frac{4\chi_0}{q_0^2} \Pi_1(\vec{Q}, \Omega)\right)} \\ &= i \frac{3}{4\pi} \text{sgn}(\omega) \int_0^{|\omega|} d\Omega \int_{-\infty}^{\infty} \frac{dk}{\left(k^2 + \sqrt{\frac{\Omega}{\bar{\omega}_0}}\right)} \\ &= i(\bar{\omega}_0)^{1/4} |\omega|^{3/4} \text{sgn}(\omega) \end{aligned} \quad (31)$$

Just as with Π_{se} , the normal state fermionic self-energy preserves the form of Eq. (20), with ω_0 replaced by $\bar{\omega}_0$. Thus, by approximating $I(x)$ as a constant ($= \alpha$), the full solution of the set of self-consistent equations for Σ and $\Pi(= \Pi_{\text{se}})$ reduces to the replacement $\omega_0 \rightarrow \bar{\omega}_0$, with no change in q_0 .

IV. SUPERCONDUCTING PROPERTIES

A. The value of T_c

The linearized gap equation (equation ((16)) without self-consistent renormalization of Σ and Π (i.e., with ω_0 instead of $\bar{\omega}_0$) has been solved by KC (Ref.²⁸). These authors obtained

$$T_c^{\text{KC}} = \omega_0 F(r) = \frac{r\bar{g}}{4\pi} F(r) \quad (32)$$

where, we remind, $r = \bar{g}\beta^2 / (\pi v_F^2)$ is the dimensionless parameter proportional to the FS curvature. The function $F(r)$ is a non-monotonic function of r , with a flat maximum near $r \sim 10^{-1}$. Using $\bar{g} \sim 1.6$ eV (extracted from the charge transfer gap) and $t - t'$ dispersion with parameters taken from ARPES, KC obtained $\omega_0 \sim 10$ meV and $r \sim 0.08$, with $F(r) \sim 0.1$ (Ref.²⁸). This yields $T_c^{\text{KC}} \sim 10$ K.

As we just discussed, the self-consistency of Σ and Π changes the scale ω_0 into $\bar{\omega}_0 = \omega_0 / \alpha^2$, with $\alpha \sim 0.6$. The static part of the susceptibility in (17), which provides the r -contribution in $F(r)$, is not affected by this renormalization, i.e., $F(r)$ does not change. We then obtain,

$$T_c(r) = \bar{\omega}_0 F(r) = \frac{T_c^{\text{KC}}}{\alpha^2} \sim 3T_c^{\text{KC}}. \quad (33)$$

so that T_c changes by a factor of about 3. For the same parameters as used by KC, we obtain $T_c \sim 30$

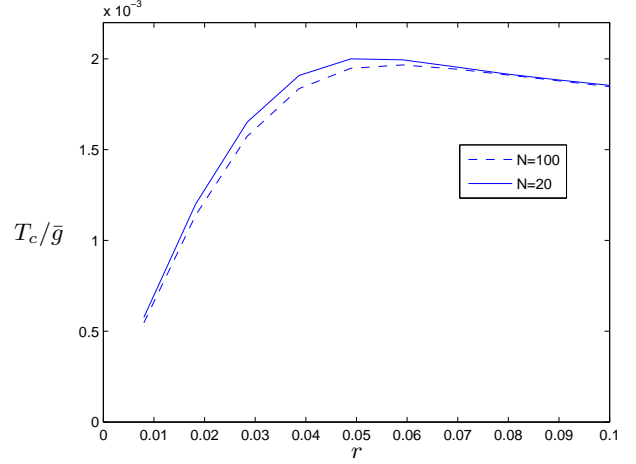


FIG. 8: T_c in units of \bar{g} versus r within the constant α approximation. The analytical formula is $T_c / \bar{g} = rF(r) / (4\pi\alpha^2)$, where $F(r)$ is a complicated function of r (see Ref.²⁸). The solid line is for $M = 20$, the dashed for $M = 100$, where M is the number of Matsubara points. The two curves are in good agreement, thus providing a check on our solution. We kept the number of points for the Gauss-Legendre (GL) quadrature fixed at $M_{\text{GL}} = 10$.

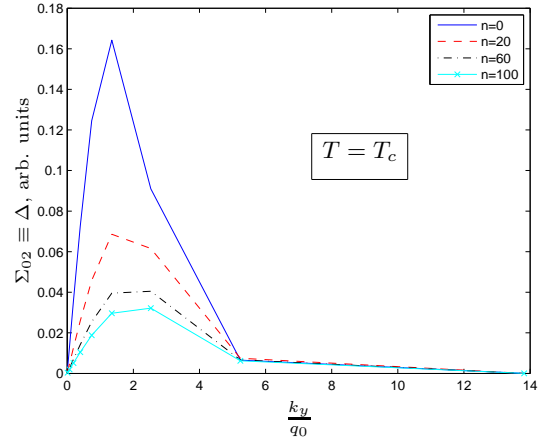


FIG. 9: $\Sigma_{02}(k_y, \omega_n)$ versus k_y / q_0 , obtained as a normalized eigenvector of the linearized gap equation. We set $r = 0.08$ ($T_c \sim 0.30\omega$). The magnitude of this Σ_{02} does not have any significance as the actual Σ_{02} is infinitesimally small at T_c . The n in the legend correspond to different Matsubara frequencies, ω_n .

K. For completeness we also computed $T_c(r)$ and the eigenfunction $\Delta(k_y, \omega_n)$ numerically, within our constant α approximation. We used the Gauss-Legendre quadrature method, one of the many Gaussian type quadrature approximations³². We present the result for $T_c(r)$ in Fig. 8. We find that the functional form of $T_c(r)$ is quite similar to the one obtained by KC, and the values are about 3 times larger than theirs, as expected. We also emphasize

that $T_c(r)$ is rather flat over a wide range of $r \leq 10^{-1}$, so that any inaccuracy in determining the value of r has little effect on T_c .

Our result is in much better agreement with experiments than T_c^{KC} , particularly given that hot spot calculations tend to somewhat overestimate the value of T_c compared to full scale calculation without expanding the fermionic dispersion near the hot spots²⁹.

In Fig. 9 we present the eigenfunction of the linearized gap equation for various Matsubara frequencies. It shows that the infinitesimally small d -wave gap at T_c is non-monotonic along the FS, with its maximum not at the hot spot (the point $k_y = 0$) but at a point away from it. This agrees with the result of KC.

B. The non-linear gap equation

We next derive and solve the non-linear gap equation for $T < T_c$. The key goals here are to obtain the an-

gular dependence of the gap along the FS, and to verify whether it remains non-monotonic below T_c . In the process, we also obtain the frequency dependence of the gap and compute the ratio $2\Delta_{\text{max}}/T_c$.

The computational procedure is straightforward. We introduce $\Delta(\vec{k}, \omega_n)$ and fermionic $Z(\vec{k}, \omega_n)$ via

$$\Sigma(\vec{k}, \omega_n) = -i\omega_n(1 - Z(\vec{k}, \omega_n)) \quad (34)$$

$$\Delta(\vec{k}, \omega_n) = \Sigma_{02}(\vec{k}, \omega_n)/Z(\vec{k}, \omega_n). \quad (35)$$

The equations for the normal and anomalous, fermionic self-energies are re-expressed via Δ and Z as

$$Z(p) = 1 + \frac{3g^2T}{i\omega_n} \sum_m \int \frac{d^2\vec{k}}{(2\pi)^2} \frac{i\omega_m Z(\vec{k}, \omega_m) + \epsilon_k}{(\omega_m^2 + \Delta(\vec{k}, \omega_m)^2)Z(\vec{k}, \omega_m)^2 + \epsilon_k^2} \chi(\vec{k} - \vec{p}, \omega_m - \omega_n) \quad (36a)$$

$$\Sigma_{02}(p) = \Delta(p)Z(p) = 3g^2T \sum_m \int \frac{d^2\vec{k}}{(2\pi)^2} \frac{\Delta(\vec{k}, \omega_m)Z(\vec{k}, \omega_m)}{(\omega_m^2 + \Delta(\vec{k}, \omega_m)^2)Z(\vec{k}, \omega_m)^2 + \epsilon_k^2} \chi(\vec{k} - \vec{p}, \omega_m - \omega_n) \quad (36b)$$

where $p = (\vec{p}, \omega_n)$. We restrict momenta in Δ to the Fermi surface and introduce

$$\Delta(\vec{p}, \omega_m)|_{\epsilon_p=0} = \Delta(p_y, \omega_m) \quad (37)$$

Carrying out the integration w.r.t. ϵ_k as before, and using Eq. (36a) to eliminate Z in the l.h.s. of Eq. (36b), we obtain the non-linear gap equation in the form

$$\Delta(\tilde{p}, \omega_n) = \frac{\frac{3T}{4\tilde{\omega}_0^N} \sum_m \int_{-\infty}^{\infty} d\tilde{k} \frac{\tilde{\chi}(\tilde{p}, \tilde{k}, \omega_n - \omega_m)}{\sqrt{\omega_m^2 + \Delta^2(\tilde{k}, \omega_m)}} \Delta(\tilde{k}, \omega_m)}{1 + \frac{3T}{4\tilde{\omega}_0^N} \sum_m \int_{-\infty}^{\infty} d\tilde{k} \frac{2m+1}{2n+1} \frac{\tilde{\chi}(\tilde{p}, \tilde{k}, \omega_m - \omega_n)}{\sqrt{(\omega_m^2 + \Delta^2(\tilde{k}, \omega_m))}}} \quad (38)$$

where we have

$$\tilde{\chi}(\tilde{p}, \tilde{k}, \Omega_n) = \frac{1}{\left((\tilde{p} - \tilde{k})^2 + r^2(\tilde{p}^2 + \tilde{k}^2)^2 + \tilde{\Pi}_{\text{tot}}(\vec{Q}, \Omega_n) \right)}, \quad (39)$$

and we introduced dimensionless $\tilde{k} = k_y/q_0$, $\tilde{p} = p_y/q_0$, and $\tilde{\Pi}_{\text{tot}} = (\chi_0/q_0^2)\Pi_{\text{tot}} = (4\chi_0/q_0^2)\Pi$. The full polarization operator depends on $\Delta(\vec{k}, \omega_n)$ and is given by

$$\tilde{\Pi}_{\text{tot,sc}}(\vec{Q}, \Omega_n) = -\frac{2T}{\tilde{\omega}_0^N} \sum_m \int_{-\infty}^{\infty} d\tilde{k} (E_1 + E_2 + E_3) \quad (40)$$

where

$$\begin{aligned}
E_1 &= -i \left(1 + \frac{\omega_m}{\sqrt{\omega_m^2 + \Delta^2(\tilde{k}, \omega_m)}} \right) \frac{8\tilde{k}^2 + i \left((\omega_m + \Omega_n) - \sqrt{\omega_m^2 + \Delta^2(\tilde{k}, \omega_m)} \right)}{(8\tilde{k}^2 - i\sqrt{\omega_m^2 + \Delta^2(\tilde{k}, \omega_m)})^2 + ((\omega_m + \Omega_n)^2 + \Delta^2(\tilde{k}, \omega_m + \Omega_n))} \\
E_2 &= i \left(1 - \frac{\omega_m + \Omega_n}{\sqrt{(\omega_m + \Omega_n)^2 + \Delta^2(\tilde{k}, \omega_m + \Omega_n)}} \right) \frac{8\tilde{k}^2 + i \left(\omega_m + \sqrt{(\omega_m + \Omega_n)^2 + \Delta^2(\tilde{k}, \omega_m + \Omega_n)} \right)}{(8\tilde{k}^2 + i\sqrt{(\omega_m + \Omega_n)^2 + \Delta^2(\tilde{k}, \omega_m + \Omega_n)})^2 + (\omega_m^2 + \Delta^2(\tilde{k}, \omega_m))} \\
E_3 &= \Delta(\tilde{k}, \omega_m) \Delta(\tilde{k}, \omega_m + \Omega_n) \left(\frac{1}{\sqrt{\omega_m^2 + \Delta^2(\tilde{k}, \omega_m)} \left((8\tilde{k}^2 - i\sqrt{\omega_m^2 + \Delta^2(\tilde{k}, \omega_m)})^2 + ((\omega_m + \Omega_n)^2 + \Delta^2(\tilde{k}, \omega_m + \Omega_n)) \right)} + \right. \\
&\quad \left. \frac{1}{\sqrt{(\omega_m + \Omega_n)^2 + \Delta^2(\tilde{k}, \omega_m + \Omega_n)} \left((8\tilde{k}^2 + i\sqrt{(\omega_m + \Omega_n)^2 + \Delta^2(\tilde{k}, \omega_m + \Omega_n)})^2 + (\omega_m^2 + \Delta^2(\tilde{k}, \omega_m)) \right)} \right)
\end{aligned} \tag{41}$$

Eqs. (38) and (40) have to be solved self-consistently for $T < T_c$, to obtain the superconducting gap $\Delta(\vec{k}_F, \omega_n)$ along the Fermi surface.

C. Numerical solution of the non-linear gap equation

We numerically solve the above set of equations using the Gauss-Legendre quadrature. We choose a particular value of $r \sim 0.08$ for which $T_c \sim 0.10 \bar{\omega}_0 \sim 0.30 \omega_0$.

In Fig. 10 we present our results for the solution of the coupled non-linear equations (38) and (40), for various $T < T_c$. We see that the gap continues to be non-monotonic along the FS for all Matsubara frequencies, with its magnitude increasing as T decreases, as indeed it should. The position of the maximum remains essentially intact. We consider our results as proof that the gap in electron-doped cuprates is indeed non-monotonic along the FS. We emphasize that the position of the maximum is *not* at hot spots, which in our approximation are located right where the zone diagonals intersect the FS.

In Fig. 11, we plot the temperature dependence of the gap maximum, at different Matsubara frequencies, measured in units of T_c . We see that for the lowest Matsubara frequency ($n = 0$) the ratio

$$\frac{2\Delta_{\max}(T \rightarrow 0, n = 0)}{T_c} \sim 4 \tag{42}$$

The $n = 0$ value of $\Delta(\vec{k}_F, \omega_n)$ is close to the real frequency $\omega = 0$ value of the gap; so we predict that the ratio of the measured largest 2Δ along the FS and T_c should be close to four. This is not far from the BCS result for a d -wave superconductor³³. Experimentally, from

optics we have³¹ $2\Delta_{\max}/T_c \sim 5$ for $\text{Pr}_{1.85}\text{Ce}_{0.15}\text{CuO}_4$, and from Raman measurements⁵ on $\text{Pr}_{2-x}\text{Ce}_x\text{CuO}_4$ and $\text{Nd}_{2-x}\text{Ce}_x\text{CuO}_4$ we have $2\Delta_{\max}/T_c \sim 3.5$.

V. SUMMARY DISCUSSION

To summarize, we have considered in this paper normal state properties, the pairing instability temperature, and the structure of the pairing gap in electron-doped cuprates. We assumed that the pairing is mediated by low-energy, collective spin excitations, and that antiferromagnetic order develops close to the doping where the FS touches the magnetic Brillouin zone boundary at four points, hot spots, which at this doping lie on the zone diagonals (i.e., antiferromagnetism emerges together with the appearance of hot spots).

Because of the absence of a natural ω_D/E_F parameter, we extended the low-energy spin-fermion model, using Eliashberg theory, to $N \gg 1$ fermionic flavors with $1/N$ a small parameter. Using this we justified the neglect of vertex corrections and of $d\Sigma(k)/d\epsilon_k$; and also argued for the necessity to solve self-consistently, in the normal state, the coupled integral equations for fermionic $\Sigma(\omega)$ and bosonic $\Pi(\vec{Q}, \Omega)$. This is necessary because the self-energy corrections to the polarization bubble are not small in $1/N$. In this respect, Eliashberg theory in electron-doped cuprates is different from the one in hole-doped cuprates. In hole-doped systems, the hot spots are far from the zone diagonals, Fermi velocities at hot spots separated by \vec{Q} are directed at a finite angle w.r.t. each other, and the polarization bubble, $\Pi(\vec{Q}, \Omega) \propto |\Omega|$, is the convolution of local Green's functions which do not depend on the self energy $\Sigma(\omega)$. In electron-doped cuprates, the hot spots at QCP are on the zone diagonals,

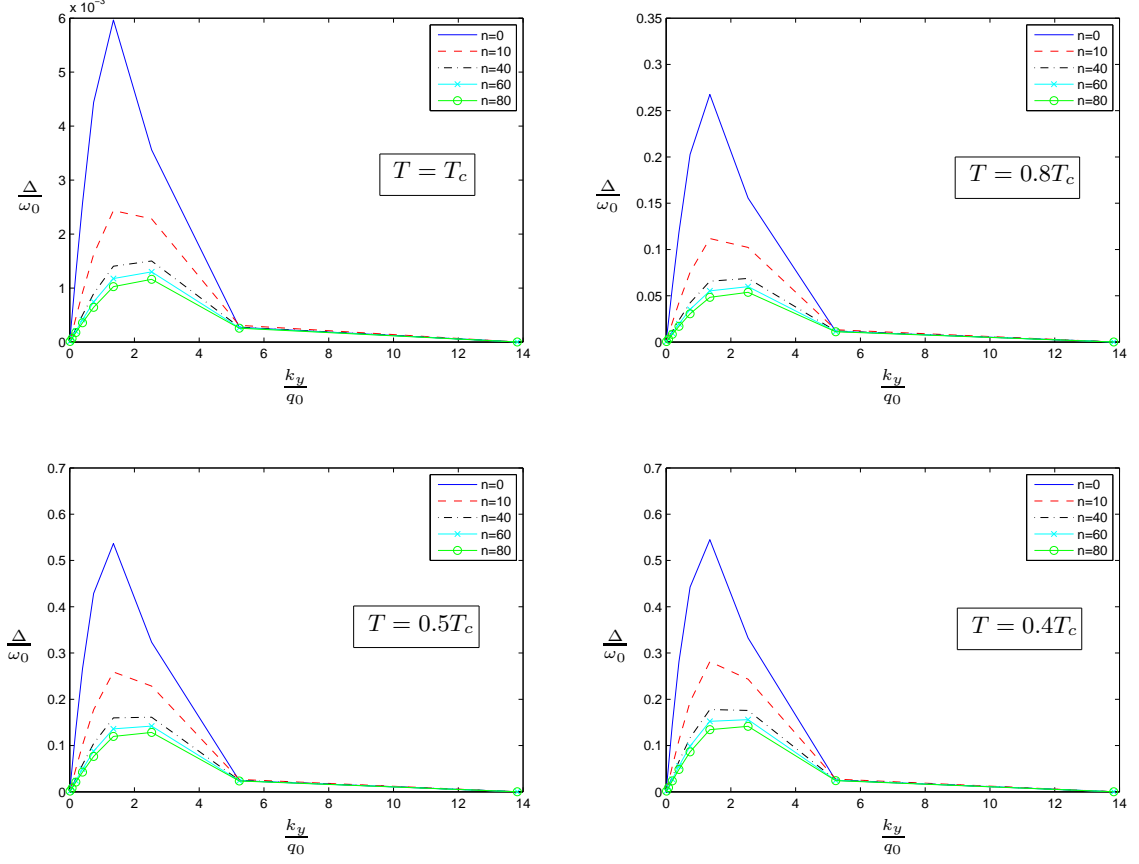


FIG. 10: The superconducting gap $\Delta(k_y, \omega_n)$ (in units of ω_0) obtained as a solution of the non-linear gap equation for different temperatures $T \leq T_c$. We set $r \sim 0.08$ ($T_c \sim 0.30\omega_0$) The index n in the legend correspond to different Matsubara frequencies ω_n .

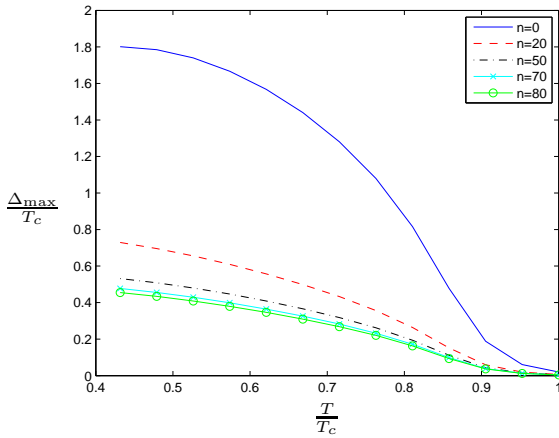


FIG. 11: The momentum peak of $\Delta(k_y, \omega_n)$ in units of T_c , plotted against T/T_c . Parameters are the same as in Fig. 10.

the velocities of fermions separated by \vec{Q} are antiparallel, and the polarization bubble $\Pi(\vec{Q}, \Omega) \propto \sqrt{|\Omega|}$ is not expressed as a convolution of two local Green's functions. As a consequence, the self-energy corrections become relevant, necessitating a self-consistent analysis of $\Pi(\vec{Q}, \Omega)$ and $\Sigma(\omega)$.

In the earlier study by KC²⁸, these self-energy corrections to the bubble were not included, and the T_c calculation was carried out without taking this self-consistency into account. In our work we have computed Σ and Π self-consistently. We have argued that, to a reasonable accuracy, the self-consistent solution for Σ and Π reduces to the renormalization of earlier results by constant factors, i.e., $\Pi \rightarrow \alpha\Pi$ and $\Sigma \rightarrow \Sigma/\sqrt{\alpha}$, where $\alpha \sim 0.6$.

Using these results, we re-derived the formula for T_c and obtained $T_c \rightarrow T_c/\alpha^2 \sim 3T_c$. Using the same parameters as in the earlier study, we obtained $T_c \sim 30 - 35\text{K}$, in very good agreement with the experimental data for electron-doped cuprates.

We then derived a coupled set of non-linear equations,

for $T < T_c$, for the frequency and momentum dependent d -wave superconducting gap $\Delta(\vec{k}_F, \omega_n)$ along the FS and the polarization operator $\Pi(\vec{Q}, \Omega_n)$. These equations are highly non-linear as Δ holds non-linear dependence on Π , and Π holds non-linear dependence on Δ . Our numerical solution of this set of non-linear equations shows that $\Delta(\vec{k}_F, \omega_n)$ decreases monotonically, as expected, with increasing Matsubara frequency ω_n ; and more interestingly, that for each ω_n the gap is non-monotonic in momentum along the FS, with its node at the zone diagonal (where a hot spot is also located), and the maximum some distance away from the zone diagonal. This non-monotonicity of the superconducting gap has been conjectured based on the analysis of Raman data⁴ and subsequently detected in ARPES measurements.⁹

For $2\Delta_{\max}(T \rightarrow 0, n = 0)/T_c$ we obtained a value close to four. This is also consistent with the data: from op-

tical measurements $2\Delta_{\max}/T_c \sim 5$ (Ref.³¹), and from Raman measurements $2\Delta_{\max}/T_c \sim 3.5$ (Ref.⁵).

VI. ACKNOWLEDGEMENTS

We acknowledge helpful discussions with Mark Friesen, Ilya Eremin, James Rossmanith, and Tigran Sedrakyan. This work was supported by NSF-DMR-0906953.

Appendix A: Calculation of Π_v

In this appendix we present the details of the calculation of the polarization operator with a vertex correction, Eq. (21). We have

$$\Pi_v(\vec{Q}, \Omega) = -2Ng^4 \int_{-\infty}^{\infty} \frac{d\omega d^2\mathbf{k} d\omega' d^2\mathbf{k}'}{(2\pi)^6} \frac{\chi(\vec{k} - \vec{k}', \omega - \omega')}{(i\omega - \epsilon_{\mathbf{k}})(i(\omega + \Omega) - \epsilon_{\mathbf{k}+\mathbf{Q}})(i\omega' - \epsilon_{\mathbf{k}'})(i(\omega' + \Omega) - \epsilon_{\mathbf{k}'+\mathbf{Q}})} \quad (\text{A1})$$

Using Eqs. (3) and (4) for $\epsilon_{\mathbf{k}}$ and $\epsilon_{\mathbf{k}+\mathbf{Q}}$ and carrying out a change of variables, we re-write (A1) as

$$\Pi_v(\vec{Q}, \Omega) = -\frac{2Ng^4}{v_F^2} \int_{-\infty}^{\infty} \frac{d\omega d\omega' dk_y dk'_y d\epsilon_{\mathbf{k}} d\epsilon_{\mathbf{k}'}}{(\epsilon_{\mathbf{k}} - i\omega)(\epsilon_{\mathbf{k}} - 2\beta^2 k_y^2 + i(\omega + \Omega))(\epsilon_{\mathbf{k}'} - i\omega')(\epsilon_{\mathbf{k}'} - 2\beta^2 k_y'^2 + i(\omega' + \Omega))} \chi(\vec{k}' - \vec{k}, \omega' - \omega) \quad (\text{A2})$$

Once again, neglecting the dependence of χ on $\epsilon_{\mathbf{k}}$, we set,

$$\chi(\vec{k}' - \vec{k}, \omega' - \omega) = \chi(\vec{k}' - \vec{k}, \omega' - \omega)|_{\epsilon_{\mathbf{k}} = \epsilon_{\mathbf{k}'} = 0} \quad (\text{A3})$$

Using equation (8) for χ , and eliminating the dependence on k_x, k'_x using

$$\begin{aligned} \epsilon_{\mathbf{k}} &= v_F k_x + \beta^2 k_y^2 = 0 \\ \epsilon_{\mathbf{k}'} &= -v_F k'_x + \beta^2 k_y'^2 = 0 \end{aligned} \quad (\text{A4})$$

we obtain,

$$\begin{aligned} \chi(k'_y, k_y, \omega' - \omega) &= \chi(\vec{k}' - \vec{k}, \omega' - \omega)|_{\epsilon_{\mathbf{k}} = \epsilon_{\mathbf{k}'} = 0} \\ &= \frac{\chi_0}{(k_y - k'_y)^2 + \frac{\beta^4}{v_F^2} (k_y^2 + k_y'^2)^2 + 4\chi_0 \Pi(\vec{Q}, \omega' - \omega)} \\ &= \frac{\chi_0}{q_0^2 \left((k - k')^2 + r^2 (k^2 + k'^2)^2 + N \sqrt{\frac{|\omega' - \omega|}{\omega_0}} \right)}. \end{aligned} \quad (\text{A5})$$

In the last line we have replaced k_y and k'_y by dimensionless $k = k_y/q_0$ and $k' = k'_y/q_0$, and used Eq. (19) for Π with $F_{\Pi} = 1$ because we are at $T \rightarrow 0$. Also the ω_0 that appears is as given by equation (7), i.e. without the large N redefinition. We have verified that for the present calculation the r dependent term in χ is irrelevant and can be dropped. The integrations w.r.t. $\epsilon_{\mathbf{k}}, \epsilon_{\mathbf{k}'}$ are factorized and easy to carry out. The result is

$$\begin{aligned} \Pi_v(\vec{Q}, \Omega) = & -\frac{2Ng^4}{v_F^2(2\pi)^6} \int dk_y dk'_y \left[2\pi i \int_0^\infty \frac{d\omega}{i(2\omega + \Omega) - 2\beta^2 k_y^2} + 2\pi i \int_{-\infty}^{-\Omega} \frac{d\omega}{2\beta^2 k_y^2 - i(2\omega + \Omega)} \right] \\ & \left[2\pi i \int_0^\infty \frac{d\omega'}{i(2\omega' + \Omega) - 2\beta^2 k'_y{}^2} + 2\pi i \int_{-\infty}^{-\Omega} \frac{d\omega'}{2\beta^2 k'_y{}^2 - i(2\omega' + \Omega)} \right] \chi(k'_y - k_y, \omega' - \omega) \end{aligned} \quad (\text{A6})$$

Re-arranging the integrals over $d\omega$ and $d\omega'$, we get a more compact result

$$\Pi_v(\vec{Q}, \Omega) = \frac{2Ng^4}{(2\pi)^4} \int dk_y dk'_y \left(\int_0^\infty d\omega d\omega' - \int_0^\infty d\omega \int_{-\infty}^{-\Omega} d\omega' \right) (D(\omega, k_y) D(\omega', k'_y) + \text{c.c.}) \chi(k'_y - k_y, \omega' - \omega) \quad (\text{A7})$$

where

$$D(\omega, k_y) = \frac{1}{2\beta^2 k_y^2 - i(2\omega + \Omega)} \quad (\text{A8})$$

and

$$D(\omega, k_y) D(\omega', k'_y) + \text{c.c.} = 2 \frac{2\beta^2 k_y^2 2\beta^2 k'_y{}^2 - (2\omega + \Omega)(2\omega' + \Omega)}{((2\beta^2 k_y^2)^2 + (2\omega + \Omega)^2)((2\beta^2 k'_y{}^2)^2 + (2\omega' + \Omega)^2)} \quad (\text{A9})$$

Substituting this into (A7) and using $2\beta^2 k^2 = 8\omega_0 k^2$, where k is the dimensionless variable introduced above, we obtain

$$\begin{aligned} \Pi_v(\vec{Q}, \Omega) = & \frac{g^2}{2\pi\beta v_F} \frac{\sqrt{\omega_0}}{64\pi^2} \left(\int_0^\infty d(\omega/\omega_0) d(\omega'/\omega_0) - \int_0^\infty d(\omega/\omega_0) \int_{-\infty}^{-\Omega} d(\omega'/\omega_0) \right) \\ & \int dk dk' \frac{F_\Omega(k, k', \omega, \omega')}{(k - k')^2 + N\sqrt{|\omega - \omega'|/\omega_0}} \end{aligned} \quad (\text{A10})$$

where

$$F_\Omega(k, k', \omega, \omega') = \frac{k^2 k'^2 - \left(\frac{2\omega + \Omega}{8\omega_0}\right) \left(\frac{2\omega' + \Omega}{8\omega_0}\right)}{(k^4 + \left(\frac{2\omega + \Omega}{8\omega_0}\right)^2)(k'^4 + \left(\frac{2\omega' + \Omega}{8\omega_0}\right)^2)} \quad (\text{A11})$$

Extending this result to large N as described in the main text (Eq. (18)), i.e., redefining $\omega_0 \rightarrow \omega_0/N^2$; and introducing new variables

$$x = \omega/\omega_0, \quad y = \omega'/\omega_0 \quad (\text{A12})$$

and

$$\bar{k} = Nk, \quad \bar{k}' = Nk' \quad (\text{A13})$$

we obtain

$$\begin{aligned} \Pi_v(\vec{Q}, \Omega) = & \frac{N^2 g^2}{2\pi\beta v_F} \frac{\sqrt{\omega_0}}{64\pi^2} \left(\int_0^\infty dx dy - \int_0^\infty dx \int_{-\infty}^{-\Omega} dy \right) \\ & \int d\bar{k} d\bar{k}' \frac{\bar{k}^2 \bar{k}'^2 - AB}{(\bar{k}^4 + A^2)(\bar{k}'^4 + B^2)((\bar{k} - \bar{k}')^2 + 2N^2 \sqrt{|A - B|})} \end{aligned} \quad (\text{A14})$$

where

$$\begin{aligned} A &= \frac{2x + \Omega'}{8} \\ B &= \frac{2y + \Omega'}{8} \end{aligned} \quad (\text{A15})$$

and

$$\Omega' = \frac{\Omega}{\omega_0}, \quad (\text{A16})$$

Rearranging the limits of integration in the second set of x, y integrations, we obtain,

$$\begin{aligned} \Pi_v(\vec{Q}, \Omega) = & \frac{N^2 g^2 \sqrt{\omega_0}}{2\pi\beta v_F 64\pi^2} \int_0^\infty dx dy \int d\bar{k} d\bar{k}' \frac{\bar{k}^2 \bar{k}'^2 - AB}{(\bar{k}^4 + A^2)(\bar{k}'^4 + B^2)((\bar{k} - \bar{k}')^2 + 2N^2\sqrt{|A-B|})} \\ & - \frac{\bar{k}^2 \bar{k}'^2 + AB}{(\bar{k}^4 + A^2)(\bar{k}'^4 + B^2)((\bar{k} - \bar{k}')^2 + 2N^2\sqrt{|A+B|})} \end{aligned} \quad (\text{A17})$$

Performing the integration over \bar{k} and \bar{k}' we obtain, after some algebra,

$$\begin{aligned} \Pi_v(\vec{Q}, \Omega) = & \frac{N^2 g^2 \sqrt{\omega_0}}{2\pi\beta v_F} \frac{1}{64} \int_0^\infty dx dy \left(\frac{|\sqrt{A} - \sqrt{B}|}{\sqrt{AB}(4N^4(\sqrt{A} + \sqrt{B}) + |\sqrt{A} - \sqrt{B}|^3)} \right. \\ & - \frac{A - B + 2N^2\sqrt{|A-B|}}{2N\sqrt{B}\sqrt{\sqrt{|A-B|}} \left(\left(A - B - 2N\sqrt{B}\sqrt{\sqrt{|A-B|}} \right)^2 + 4N^2\sqrt{|A-B|}(N\sqrt{\sqrt{|A-B|}} + \sqrt{B})^2 \right)} \\ & - \frac{B - A + 2N^2\sqrt{|A-B|}}{2N\sqrt{A}\sqrt{\sqrt{|A-B|}} \left(\left(B - A - 2N\sqrt{A}\sqrt{\sqrt{|A-B|}} \right)^2 + 4N^2\sqrt{|A-B|}(\sqrt{A} + N\sqrt{\sqrt{|A-B|}})^2 \right)} \\ & - \frac{2(\sqrt{AB} + N^2\sqrt{A+B})}{\sqrt{AB}((A+B)^2 + 4N^4(A+B) + 8N^2\sqrt{AB}\sqrt{A+B})} \\ & - \frac{A + B - 2N^2\sqrt{A+B}}{2N\sqrt{B}\sqrt{\sqrt{A+B}} \left(\left(A + B + 2N\sqrt{B}\sqrt{\sqrt{A+B}} \right)^2 + 4N^2\sqrt{A+B}(\sqrt{B} + N\sqrt{\sqrt{A+B}})^2 \right)} \\ & \left. - \frac{A + B - 2N^2\sqrt{A+B}}{2N\sqrt{A}\sqrt{\sqrt{A+B}} \left(\left(A + B + 2N\sqrt{A}\sqrt{\sqrt{A+B}} \right)^2 + 4N^2\sqrt{A+B}(\sqrt{A} + N\sqrt{\sqrt{A+B}})^2 \right)} \right) \end{aligned} \quad (\text{A18})$$

We note that our result is symmetric w.r.t. to $A \leftrightarrow B$ as it should be, since the original integrals are symmetric w.r.t. $\omega \leftrightarrow \omega'$. Evaluating the remaining integrals, subtracting the Ω -independent term coming from large x, y (i.e., from high internal frequencies), and taking large N limit, we find the leading term to be

$$\Pi_v(\vec{Q}, \Omega) = \frac{g^2 \sqrt{\omega_0}}{2\pi\beta v_F} \frac{1}{2} \sqrt{\frac{\Omega'}{8}} \log \left(2N^2 \sqrt{\frac{8}{\Omega'}} \right) \quad (\text{A19})$$

This is the result we quoted in the main text, Eq. (22).

¹ J. Bednorz, and K. A. Muller, Z. Phys. B 64, 189 (1986).

² H. Takagi, S. Uchida, and Y. Tokura, Phys. Rev. Lett. 62, 1197 (1989).

³ N. P. Armitage, P. Fournier, and R. L. Greene, Rev. Mod. Phys. 82, 2421 (2010).

⁴ G. Blumberg, A. Koitzsch, A. Gozar, B. S. Dennis, C. A.

Kendziora, P. Fournier, and R. L. Greene, Phys. Rev. Lett. 88, 107002 (2002).

⁵ M. M. Qazilbash, A. Koitzsch, B. S. Dennis, A. Gozar, H. Balci, C. A. Kendziora, R. L. Greene, and G. Blumberg, Phys. Rev. B 72, 214510 (2005).

⁶ Z.-X. Shen and D. S. Dessau et al., Phys. Rev. Lett. 70,

- 1553 (1993).
- ⁷ H. Ding et al., Phys. Rev. B 54, 1553 (1996).
 - ⁸ N. P. Armitage, D. H. Lu, D. L. Feng, C. Kim, A. Damascelli, K. M. Shen, F. Ronning, and Z.-X. Shen, Phys. Rev. Lett. 86, 1126 (2001).
 - ⁹ H. Matsui, K. Terashima, T. Sato, T. Takahashi, S.-C. Wang, H.-B. Yang, H. Ding, T. Uefuji, and K. Yamada, Phys. Rev. Lett. 94, 047005 (2005).
 - ¹⁰ O. Fischer, Maggio-Aprile I. Kugler, I. Berthod, and C. Renner, Rev. Mod. Phys. 79, 353 (2007).
 - ¹¹ W. N. Hardy, D. A. Bonn, D. C. Morgan, R. Liang, and K. Zhang, Phys. Rev. Lett. 70, 3999 (1993).
 - ¹² J. D. Kokales, P. Fournier, L. V. Mercaldo, V. V. Talanov, R. L. Greene, and S. M. Anlage, Phys. Rev. Lett. 85, 3696 (2000).
 - ¹³ R. Prozorov, R. Giannetta, P. Fournier, and R. L. Greene, Phys. Rev. Lett. 85, 3700 (2000).
 - ¹⁴ J. A. Skinta, M.-S. Kim, T. R. Lemberger, T. Greibe, and M. Naito, Phys. Rev. Lett. 88, 207005 (2002).
 - ¹⁵ G. Deutscher, Rev. Mod. Phys. 77, 109 (2005).
 - ¹⁶ S. V. Dordevic and D. N. Basov, Ann. Phys. 15, 545 (2006).
 - ¹⁷ Y. Onose, Y. Taguchi, K. Ishizaka, and Y. Tokura, Phys. Rev. B 69, 024504 (2004).
 - ¹⁸ A. Abanov, A. V. Chubukov, and J. Schmalian, Adv. Phys. 52, 119 (2003).
 - ¹⁹ D. J. Scalapino, Phys. Rep. 250, 329 (1995).
 - ²⁰ P. Monthoux and D. Pines, Phys. Rev. B 47, 6069 (1993).
 - ²¹ D. Manske, I. Eremin, and K. H. Bennemann, Phys. Rev. B 62, 13922 (2000).
 - ²² B. Kyung, J.-S. Landry, and A.-M. S. Tremblay, Phys. Rev. B 68, 174502 (2003).
 - ²³ T. Das, R. S. Markiewicz, and A. Bansil, Phys. Rev. B 74, 020506 (2006).
 - ²⁴ P. Prelovšek and A. Ramšak, Phys. Rev. B 72, 012510 (2005).
 - ²⁵ D. J. Scalapino, E. Loh, Jr., and J. E. Hirsch, Phys. Rev. B 34, 8190 (1986).
 - ²⁶ M. T. Beal-Monod, C. Bourbonnais, and V. J. Emery, Phys. Rev. B 34, 7716 (1986).
 - ²⁷ J. Schmalian, Phys. Rev. Lett. 81, 4232 (1998).
 - ²⁸ P. Krotkov and A. V. Chubukov, Phys. Rev. B 74, 014509 (2006).
 - ²⁹ Ar. Abanov, A. V. Chubukov, and M. R. Norman, Phys. Rev. B 78, 220507 (2008).
 - ³⁰ M. A. Metlitski and S. Sachdev, Phys. Rev. B 82, 075127 (2010); Phys. Rev. B 82, 075128 (2010); D. F. Mross, J. McGreevy, H. Liu, and T. Senthil, arXiv:1003.0894; A. V. Chubukov, S.-S. Lee, and Y. B. Kim (unpublished).
 - ³¹ C. C. Homes, R. P. S. M. Lobo, P. Fournier, A. Zimmers, and R. L. Greene, Phys. Rev. B 74, 214515 (2006).
 - ³² G. W. Recktenwald, *Numerical Methods With MATLAB: Implementations and Applications* (Prentice Hall, 2000).
 - ³³ K. A. Musaelian, J. Betouras, A. V. Chubukov, and R. Joynt, Phys. Rev. B 53, 3598 (1996).